

# Stopping Light on a Defect

R.H. Goodman\* R.E. Slusher† M.I. Weinstein‡

November 20, 2018

## Abstract

*Gap solitons* are localized nonlinear coherent states which have been shown both theoretically and experimentally to propagate in periodic structures. Although theory allows for their propagation at any speed  $v$ ,  $0 \leq v \leq c$ , they have been observed in experiments at speeds of approximately 50% of  $c$ . It is of scientific and technological interest to trap gap solitons. We first introduce an explicit multiparameter family of periodic structures with localized defects, which support linear defect modes. These linear defect modes are shown to persist into the nonlinear regime, as *nonlinear defect modes*. Using mathematical analysis and numerical simulations we then investigate the capture of an incident gap soliton by these defects. The mechanism of capture of a gap soliton is resonant transfer of its energy to nonlinear defect modes. We introduce a useful bifurcation diagram from which information on the parameter regimes of gap soliton capture, reflection and transmission can be obtained by simple conservation of energy and resonant energy transfer principles.

---

\*Mathematical Sciences Research, Bell Laboratories–Lucent Technologies, Murray Hill, NJ 07974, and Program in Applied and Computational Mathematics, Princeton University, Princeton, New Jersey

†Optical Physics Research, Bell Laboratories–Lucent Technologies, Murray Hill, NJ 07974

‡Mathematical Sciences Research, Bell Laboratories–Lucent Technologies, Murray Hill, NJ 07974

# 1 Introduction

Solitons are important carriers of energy in many physical systems. The emergence of solitons is understood as a consequence of the balance of dispersive and nonlinear effects on the same length scale. Optical temporal solitons [16, 19] and more recently dispersion-managed solitons [3] have been considered candidates for the *bits* with which to transfer information over long distances. Recent advances in fabrication of optical fiber with microstructure have rendered the possibility of storing information in the form of optical *gap solitons* a natural direction for investigation.

Gap solitons are nonlinear bound states which propagate in periodic structures. These have been anticipated in theoretical work [1, 8], and observed in experiments [6, ?, 9, 18] on sufficiently high intensity light propagation in optical fiber with a periodically varying refractive index (a uniform fiber grating). In contrast to bare fiber used in long distance communications, where the formation length for solitons is on the order of kilometers, the formation length for gap solitons is on the order of centimeters. In theory, gap solitons can travel with any speed  $v$ , with  $0 \leq v \leq c$ , where  $c$  denotes the speed of light. Experiments have demonstrated the slowing of gap solitons to about 50%  $c$ .

Gap solitons propagate in fibers with uniform grating structures. In this paper we examine gratings with localized defects to the amplitude and phase of the grating. We ask whether it is possible to trap moving gap solitons at the defect location. If so, one can envision this having important technological applications, *e.g.* optical buffers or optical memory. Through a careful series of numerical experiments we show how it is possible to trap gap solitons at a defect and elucidate the mechanism by which light energy is trapped. A similar question is studied in [5] using a point-particle model for the gap soliton/defect interaction. We compare our results with the conclusions drawn in that study. Although we refer to gap soliton capture, it is perhaps better called capture of gap soliton energy, for it involves the transfer of the gap soliton's energy to a nonlinear defect mode.

This paper is laid out as follows. In Section 2, we derive a variable coefficient version of the nonlinear coupled mode equations from an appropriate one-dimensional nonlinear Maxwell model. In Section 3, we review a few facts about the gap soliton. We derive a family of defects which support linear bound states (defect modes) for the coupled mode equations in Section 4. We then examine how these bound states are deformed in the presence of

nonlinearity (nonlinear defect modes) in Section 5. The results of this study are encoded in bifurcation diagrams that display the intensity as a function of the frequency for **(a)** nonlinear defect modes and **(b)** gap solitons. With the aid of these diagrams, we develop a criterion for trapping and an understanding of its efficiency based on the notions of resonant energy transfer and energy conservation. Guided by this analysis, in Section 6, we perform a careful series of numerical experiments to show how the nonlinear bound states interact with the gap soliton to trap light energy. Simulations are carried out for the nondimensional system (2.19). Dimensional experimental parameters are displayed in Appendix A. Section 7 contains a brief discussion of the effect of nonlinear damping, a non-negligible effect in certain highly nonlinear materials, on soliton propagation and trapping. A summary and discussion of results are given in Section 8. In Appendix A we give physical parameters for silica fiber [9], discuss nondimensionalization and tabulate the dimensional values of parameters corresponding to the simulations described in Section 6. In Appendix B, we describe a method for deriving defects supporting linear bound states with prescribed characteristics.

## 2 Coupled Mode Theory in a Grating with Defects

We consider propagation of light in one dimension in an optical fiber with a refractive index which is a spatially localized perturbation about a uniformly periodic index. We model the propagation of low intensity light, confined to a core mode of the fiber by the wave equation:

$$\partial_t^2 [ n^2(z)E(z, t) ] = c^2 \partial_z^2 E, \quad (2.1)$$

where the refractive index is given by:

$$n = \bar{n} + \Delta n \left( \frac{1}{2} W(z) + \nu(z) \cos(2k_B z + 2\Phi(z)) \right). \quad (2.2)$$

Here,  $\bar{n}$  denotes the refractive index of the bare fiber and  $\Delta n$ , the index contrast, is assumed small. The functions  $\nu$ ,  $\Phi$ , and  $W$  model the defect and are assumed to vary slowly compared to the rapid sinusoidal variation of the refractive index. A spatially localized deviation from a uniformly periodic structure of period

$$d = \pi/k_B \quad (2.3)$$

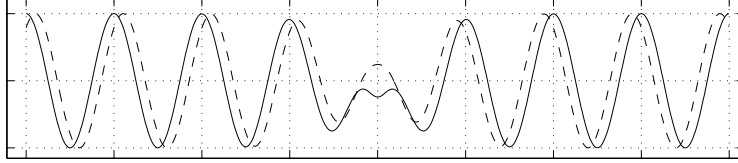


Figure 2.1: Solid and dashed curves are two different periodic index profiles with localized defects having the same “spectral characteristics” (see Section 4.2).

is obtained by taking

$$\nu(z) \rightarrow 1, \quad (2.4)$$

$$\partial_z \Phi(z) \rightarrow 0, \text{ and } \partial_z W(z) \rightarrow 0, \text{ as } |z| \rightarrow \infty. \quad (2.5)$$

Low intensity light propagating in the bare fiber ( $\Delta n = 0$ ) is governed by the spatially homogeneous linear wave equation which supports independently propagating, forward and backward plane wave solutions  $E_{\pm} e^{i(kz - \omega t)}$ , where

$$\omega = \pm \frac{ck}{\bar{n}}. \quad (2.6)$$

The periodic structure ( $\Delta n \neq 0$ ) couples these backward and forward components. This effect is most pronounced for wavelengths in the medium at or near  $\lambda = 2d$  or equivalently the (free space) *Bragg wavelength*

$$\lambda_B = 2\bar{n}d. \quad (2.7)$$

For modeling propagation in the nonlinear regime we assume an instantaneous nonlinear polarization [2]:

$$P_{\text{NL}} = \epsilon_0 \chi^{(3)} E^3. \quad (2.8)$$

Combining this with (2.2), the squared index of refraction with linear and nonlinear effects included is then

$$n^2(z, E^2) = \bar{n}^2 + \bar{n} \Delta n W(z) + 2\bar{n} \Delta n \nu(z) \cos(2k_B z + 2\Phi(z)) + \chi^{(3)} E^2. \quad (2.9)$$

For high intensities the electric field evolves under the nonlinear wave equation<sup>1</sup>:

$$\partial_t^2 [n^2(z, E^2) E] = c^2 \partial_z^2 E. \quad (2.10)$$

So that we can systematically obtain equations of evolution for the forward and backward carrier wave envelopes, we make explicit our assumptions on the medium. We assume that the variation of the refractive index is weak, and that the deviation from periodicity is small, *i.e.* there exists a small parameter  $\varepsilon \ll 1$  such that:

$$\begin{aligned} \Delta n &= \mathcal{O}(\varepsilon), \\ \partial_z W &= \mathcal{O}(\varepsilon), \partial_z \nu = \mathcal{O}(\varepsilon), \partial_z \Phi = \mathcal{O}(\varepsilon), \text{ and } \partial_z^2 \Phi = \mathcal{O}(\varepsilon^2). \end{aligned}$$

Due to the periodic structure, we expect coupling of forward and backward wave components. This coupling is strongest if the wavelength and period are chosen according to the above Bragg condition. We now make a *multiple scales ansatz*, choosing the carrier wavenumber in *Bragg resonance* with the medium:

$$E = e_+(z, t)e^{i(k_B z + \Phi - \omega_B t)} + e_-(z, t)e^{-i(k_B z + \Phi + \omega_B t)} + E_1, \quad (2.11)$$

where the wavenumber  $k_B$  and frequency  $\omega_B$  satisfy the dispersion relation

$$\omega_B = \frac{ck_B}{\bar{n}};$$

see for example [15]. The first two terms in (2.11) consist of slowly modulated forward and backward waves. The regime we consider is specified by the above assumptions on the medium and assumptions on the field amplitude, which we take to satisfy:

$$\chi^{(3)}|E|^2 = \mathcal{O}(\varepsilon).$$

---

<sup>1</sup>We work with the model (2.9)–(2.10) since it yields a simple derivation of the envelope equations (2.13). The situation is however a bit more complicated. Although (2.9)–(2.10) incorporates the effects of photonic band dispersion, this alone is insufficient to arrest optical carrier shock formation on the relevant temporal and spatial scales [15]. In fact, a valid envelope description in the absence of material dispersion would require the incorporation of coupling to *all* higher harmonics since they are in resonance.

The latter ensures a balance of nonlinearity and *photonic band dispersion* due to the periodic structure. We therefore anticipate that the amplitudes  $e_{\pm}$  will be slowly varying and will satisfy:

$$\begin{aligned}\partial_t e_{\pm} &= \mathcal{O}(\varepsilon), \quad \partial_z e_{\pm} = \mathcal{O}(\varepsilon), \\ \partial_t^2 e_{\pm} &= \mathcal{O}(\varepsilon^2), \quad \partial_z^2 e_{\pm} = \mathcal{O}(\varepsilon^2),\end{aligned}$$

The envelope functions  $e_{\pm}$  in (2.11) are finally determined by the constraint that the correction terms are of higher order in  $\varepsilon$  over a time scale and length scale of order  $\mathcal{O}(\varepsilon^{-1})$ ,

$$E_1/e_{\pm} = \mathcal{O}(\varepsilon). \quad (2.12)$$

The condition (2.12) requires the removal of resonant forcing terms in the equation for  $E_1$ . This is equivalent to the constraint that  $e_{\pm}$  satisfy the variable coefficient nonlinear coupled mode equations:

$$\begin{aligned}i\frac{\bar{n}}{c}\partial_t e_+ + i\partial_z e_+ + \tilde{V}(z)e_+ + \tilde{\kappa}(z)e_- + \tilde{\Gamma}(|e_+|^2 + 2|e_-|^2)e_+ &= 0 \\ i\frac{\bar{n}}{c}\partial_t e_- - i\partial_z e_- + \tilde{V}(z)e_- + \tilde{\kappa}(z)e_+ + \tilde{\Gamma}(|e_-|^2 + 2|e_+|^2)e_- &= 0.\end{aligned} \quad (2.13)$$

The coefficient functions in (2.13) are defined in terms of the parametric functions which characterize the index profile (2.2).<sup>2</sup>

$$\tilde{\kappa}(z) = \frac{\pi\Delta n}{\lambda_B}\nu(z) \quad (2.14)$$

$$\tilde{V}(z) = \frac{\pi\Delta n}{\lambda_B}W(z) - \Phi'(z) \quad (2.15)$$

$$\tilde{\Gamma} = \frac{3\pi\chi^{(3)}}{\bar{n}\lambda_B}. \quad (2.16)$$

Our point of view is to specify grating parametric functions  $W(z)$ ,  $\nu(z)$  and  $\Phi(z)$  through the constitutive law (2.2). These determine the functions  $\tilde{\kappa}(z)$

---

<sup>2</sup>It is common to slightly redefine  $\tilde{\kappa}$  by

$$\tilde{\kappa}(z) = \eta \cdot \pi\Delta n\nu(z)/\lambda_B$$

where  $0 < \eta < 1$  is defined as an overlap integral of the radial variation of the forward and backward modes and represents the fraction of total energy in the core of the fiber.

and  $\tilde{V}(z)$ , arising in the coupled mode equations, governing the nonlinear propagation. Note the appearance of the combination of  $W$  and  $\Phi'$  in (2.15). Therefore, spectral characteristics arising due to a DC variation ( $W$ ) in the index can be, within this approximation, equivalently achieved through phase variations ( $\Phi$ ). The solid and dashed curves in Figure 2.1 are of index profiles which are equivalent in this sense; see also Section 4.2.

The assumptions on the variable coefficients guarantee that away from the defect, the system approaches the constant coefficient NLCME

$$\tilde{V}(z) \rightarrow 0 \text{ and } \tilde{\kappa}(z) \rightarrow \tilde{\kappa}_\infty \equiv \frac{\pi \Delta n}{\lambda_B}. \quad (2.17)$$

We introduce typical dimensional length,  $\mathcal{Z}$ , time,  $\mathcal{T} = \mathcal{Z}\bar{n}/c$ , and electric field,  $\mathcal{E}$ . Using these, we define *nondimensional* spatial and temporal variables  $Z$  and  $T$ , and electric field  $E_\pm$  given by:

$$z = \mathcal{Z}Z, \quad t = \frac{\mathcal{Z}\bar{n}}{c}T, \quad \text{and} \quad e_\pm = \mathcal{E}E_\pm. \quad (2.18)$$

Then (2.13) can be expressed in nondimensional form as

$$\begin{aligned} i\partial_T E_+ + i\partial_Z E_+ + \kappa(Z)E_- + V(Z)E_+ + \Gamma(|E_+|^2 + 2|E_-|^2)E_+ &= 0 \\ i\partial_T E_- - i\partial_Z E_- + \kappa(Z)E_+ + V(Z)E_- + \Gamma(|E_-|^2 + 2|E_+|^2)E_- &= 0, \end{aligned} \quad (2.19)$$

where

$$\kappa(Z) = \mathcal{Z}\tilde{\kappa}(\mathcal{Z}Z), \quad V(Z) = \mathcal{Z}\tilde{V}(\mathcal{Z}Z), \quad \text{and} \quad \Gamma = \mathcal{Z}\mathcal{E}^2\tilde{\Gamma}. \quad (2.20)$$

Our analysis and computer simulations are carried out for the nondimensional system (2.19). Conversions to dimensional form are given for important quantities in Appendix A. Note that  $\tilde{\Gamma}$  and therefore  $\Gamma$  are positive; see (2.16).

### 3 The Gap Soliton

The linearized constant coefficient NLCME ( $\kappa = \kappa_\infty$ ,  $V = 0$ ) have a “gap” in their spectrum. It has no plane-wave solutions with frequencies in the range  $(-\kappa_\infty, \kappa_\infty)$ ; see Section 4.1. The nonlinear equations support a family of traveling pulses called a gap solitons [1, 7]. The family is parameterized

by a velocity  $v$  and a detuning parameter  $\delta$  with  $|v| < 1$  and  $0 \leq \delta \leq \pi$ . It is given by:

$$\begin{aligned} E_+ &= s\alpha e^{i\eta} \sqrt{\left|\frac{\kappa_\infty}{2\Gamma}\right|} \frac{1}{\Delta} (\sin \delta) e^{is\sigma} \operatorname{sech}(\theta - i\delta/2) ; \\ E_- &= -\alpha e^{i\eta} \sqrt{\left|\frac{\kappa_\infty}{2\Gamma}\right|} \Delta (\sin \delta) e^{is\sigma} \operatorname{sech}(\theta + i\delta/2) ; \end{aligned} \quad (3.1)$$

where:

$$\begin{aligned} \gamma &= \frac{1}{\sqrt{1-v^2}} ; & \Delta &= \left(\frac{1-v}{1+v}\right)^{\frac{1}{4}} ; \\ \theta &= \gamma\kappa_\infty(\sin \delta)(z-vt) ; & \sigma &= \gamma\kappa_\infty(\cos \delta)(vz-t) ; \\ \alpha &= \sqrt{\frac{2(1-v^2)}{3-v^2}} ; & s &= \operatorname{sign}(\kappa_\infty\Gamma) \\ e^{i\eta} &= \left(-\frac{e^{2\theta} + e^{-i\delta}}{e^{2\theta} + e^{i\delta}}\right)^{\frac{2v}{3-v^2}} . \end{aligned}$$

The temporal frequency of the gap soliton is  $\kappa_\infty\gamma\cos\delta$  which is inside the band gap for  $|v| < \sin\delta$ , although in a reference frame moving at speed  $v$ , the frequency is always in the band gap. We define the maximum intensity  $I_{\max}$  and the total intensity  $I_{\text{tot}}$  and give their values for the gap soliton:

$$\begin{aligned} I_{\max} &= \max_Z (|E_+|^2 + |E_-|^2) = \frac{8\kappa_\infty\sqrt{1-v^2}}{\Gamma(3-v^2)} \sin^2 \frac{\delta}{2}, \\ I_{\text{tot}} &= \int_{-\infty}^{\infty} (|E_+|^2 + |E_-|^2) dZ = \frac{4(1-v^2)\delta}{\Gamma(3-v^2)}, \end{aligned} \quad (3.2)$$

and the full width at half-maximum (FWHM) by

$$\text{FWHM} = \frac{2\sqrt{1-v^2}}{\kappa_\infty \sin \delta} \cosh^{-1} \sqrt{1 + \cos^2 \frac{\delta}{2}}. \quad (3.3)$$

In mathematical analysis, the square root of the total intensity  $I_{\text{tot}}$  is often referred to as the  $L^2$  norm. In Figure 3.1, we plot the intensity as a function of frequency for the stationary ( $v=0$ ) gap soliton. This curve is parameterized by

$$\omega(\delta) = \kappa_\infty \cos \delta, \quad I_{\text{tot}}(\delta) = \frac{4\delta}{3\Gamma} \quad \text{for } \delta \in [0, \pi].$$

Results on linearized stability and instability of gap solitons in different parameter regimes are obtained in [4].



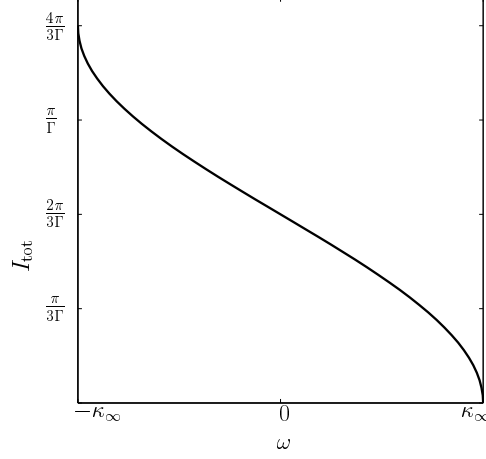


Figure 3.1: The intensity of the stationary gap soliton as a function of its frequency.

## 4 Defects and Linear Defect Modes

The functions  $V(Z)$  and  $\kappa(Z)$  define a defect in our periodic medium and we now seek the linear modes associated with this defect. These are solutions of the linear coupled mode equations:

$$i\partial_T E_+ + i\partial_Z E_+ + \kappa(Z)E_- + V(Z)E_+ = 0 \quad (4.1a)$$

$$i\partial_T E_- - i\partial_Z E_- + \kappa(Z)E_+ + V(Z)E_- = 0, \quad (4.1b)$$

or

$$[ i\partial_T + i\sigma_3\partial_Z + V(Z) + \kappa(Z)\sigma_1 ] E = 0, \quad (4.2)$$

where

$$E = \begin{pmatrix} E_+ \\ E_- \end{pmatrix}, \quad \sigma_1 = \begin{pmatrix} 0 & 1 \\ 1 & 0 \end{pmatrix}, \quad \sigma_3 = \begin{pmatrix} 1 & 0 \\ 0 & -1 \end{pmatrix}. \quad (4.3)$$

Substitution of the Ansatz

$$E(Z) = e^{-i\omega T} e^{i\sigma_3 \int_0^Z V(\zeta) d\zeta} F(Z) \quad (4.4)$$

yields

$$\partial_Z F = \begin{pmatrix} i\omega & u(Z) \\ u(Z) & -i\omega \end{pmatrix} F, \quad (4.5)$$

$$u(Z) = i\kappa(Z)e^{-2i \int_0^Z V(\zeta) d\zeta} \quad (4.6)$$

Solutions of the form (4.4), which are square integrable in  $Z$  are called *defect modes*. Solutions of the form (4.4) which are bounded and oscillatory in  $Z$  are called *radiation modes*. The set of frequencies,  $\omega$ , corresponding to defect modes and radiation modes is called the *spectrum* of (4.5).

One can pose the question: can prescribed spectral characteristics of (4.1) (*e.g.* defect modes and reflection and transmission spectra) be achieved by appropriate choice of  $u(Z)$  ( $\kappa(Z)$  and  $V(Z)$ )? This question was considered in [21] to study grating and filter design using the Gelfand-Levitan-Marchenko approach to inverse scattering; see also [23]. The Gelfand-Levitan-Marchenko method, as used in [24, 21], can be used to characterize gratings with desired spectral characteristics.

## 4.1 Radiation modes for a general localized defect

We suppose that the function  $u$  in (4.5) has the asymptotic behavior:

$$u(Z) \rightarrow \rho e^{i\theta_{\pm}}, \quad Z \rightarrow \pm\infty$$

corresponding to a spatially localized defect in the periodic structure.

The values of  $\omega$  lying in the continuous spectrum are then characterized by the equation:

$$\partial_Z F = \begin{pmatrix} i\omega & \rho e^{i\theta_{\pm}} \\ \rho e^{-i\theta_{\pm}} & -i\omega \end{pmatrix} F.$$

Seeking solutions of the form:  $e^{iQZ}\vec{v}$ , with  $Q$  real, we find that there are nontrivial solutions  $\vec{v}$  provided:

$$\omega^2 = \rho^2 + Q^2 \quad (4.7)$$

Therefore, the continuous spectrum consists of the real axis minus a gap (photonic band gap):  $-\rho < \omega < +\rho$ ; see Figure 4.1.

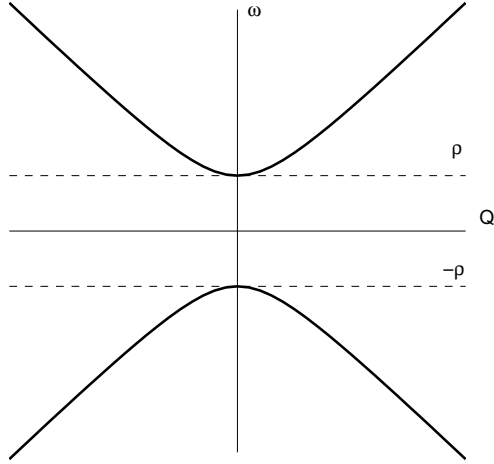


Figure 4.1: The dispersion relation (4.7), showing a band gap.

## 4.2 Dark soliton defect gratings

It is interesting to note that the system (4.5), characterizing the modes of the modulated periodic structure, is the Zakharov-Shabat eigenvalue problem associated, via the inverse scattering transform, with the *defocusing* nonlinear Schrödinger equation [24, 25]:

$$i\partial_\tau u - \partial_Z^2 u + 2|u|^2 u. \quad (4.8)$$

If  $u(Z, \tau)$  satisfies (4.8) then for each  $\tau$ , (a) the spectrum of (4.5) is independent of  $\tau$  and (b) as  $\tau$  varies, the eigenfunctions and radiation modes of (4.5) evolve in a trivial (linear) and explicitly computable manner. That is, equation (4.8) defines an isospectral deformation of the eigenvalue problem (4.5) and therefore, by (4.6), provides a rich class of potentials,  $u(Z)$ , and therefore modulated gratings  $(\kappa(Z), V(Z))$  with the same spectral characteristics.

From the inverse scattering theory of (4.8), we learn that the bound states and continuum radiation modes associated with (4.5) can be “mapped”, respectively, to the dark solitons and radiation modes of (4.8). In this section we explore those grating profiles which correspond to the simplest dark soliton solutions of (4.8).

Since the eigenvalue problem for the pair  $(F(Z), \omega)$  is self-adjoint,  $\omega$  varies over the real numbers. Furthermore, the set of all  $\omega$  satisfying  $|\omega| \geq \rho$  is *continuous spectrum*. There are no eigenvalues embedded in the continuous

spectrum. Therefore, if the eigenvalue problem (4.5) has eigenvalues they must occur in the gap  $|\omega| < \rho$ . Of interest is the following

**Inverse Problem:** Given  $N$  numbers  $\omega_1, \dots, \omega_N$ , satisfying  $|\omega_j| < \rho$ , find *potentials*,  $u(Z)$  for which these are the eigenvalues of the eigenvalue problem (4.5).

This inverse problem has many solutions. A remarkable class of solutions are those, for which the reflection coefficient associated with (4.5) is zero. These are the *dark N-soliton* solutions of defocusing NLS.

**Dark solitons (N=1):** Let  $k \neq 0$  be arbitrary and  $|\omega| < \rho$ . Let

$$\rho = |\omega + ik|.$$

Define

$$u(Z) = e^{i\phi}(\omega - ik \tanh(kZ)) \quad (4.9)$$

where  $\phi$  is left unspecified to this point.

It can be verified easily that  $\lambda$  is an eigenvalue of (4.5) with corresponding eigenfunction:

$$F(Z) = \begin{pmatrix} 1 \\ ie^{-i\phi} \end{pmatrix} \text{sech}(kZ), \quad (4.10)$$

Therefore,  $E_{\pm}$  are given by:

$$\begin{pmatrix} E_+ \\ E_- \end{pmatrix} = \begin{pmatrix} e^{\frac{i}{2} \arctan \frac{k \tanh(kZ)}{\omega}} \\ ie^{-i\phi} e^{-\frac{i}{2} \arctan \frac{k \tanh(kZ)}{\omega}} \end{pmatrix} e^{-i\omega t} \text{sech}(kZ). \quad (4.11)$$

**Specification of the grating with prescribed defect energy:**

A grating is specified by the functions  $V(Z)$  and  $\kappa(Z)$  (see (2.15) and (2.14) and (2.20)). Using (4.6) we obtain a relation between a family of “dark solitons”,  $u(Z)$ , and the functions  $V$  and  $\kappa$ :

$$i\kappa(Z)e^{-2i \int_0^Z V(s)ds} = e^{i\phi}(\omega - ik \tanh(kZ)). \quad (4.12)$$

Choosing  $\phi = \pi/2$ , this yields

$$\kappa(Z) = [\omega^2 + k^2 \tanh^2(kZ)]^{\frac{1}{2}}, \quad (4.13a)$$

$$V(Z) = \frac{1}{2}k^2 \omega [\omega^2 + k^2 \tanh^2(kZ)]^{-1} \text{sech}^2(kZ) \quad (4.13b)$$

and sets the term

$$ie^{-i\phi} = 1$$

in equations (4.10) and (4.11). Note that the limit  $\omega \rightarrow 0$  of the defect definition (4.13) is singular:

$$\kappa(Z) = |k \tanh(kZ)|, \quad (4.14a)$$

$$V(Z) = \pm \frac{\pi}{2} \delta(Z) \quad (4.14b)$$

where  $\delta(Z)$  denotes the Dirac delta function and the sign on  $V(Z)$  depends on the direction on which the limit  $\omega \rightarrow 0$  is taken. Instead, taking  $V(Z) = 0$ ,  $\omega = 0$ ,  $e^{i\phi} = \pm 1$  in equation (4.12) yields the continuous limit

$$\kappa(Z) = -k \tanh kZ \quad (4.15)$$

$$F(Z) = \begin{pmatrix} 1 \\ \mp i \end{pmatrix} \operatorname{sech} kZ \quad (4.16)$$

Recall that in our coupled mode system, the medium is characterized by three functions:  $\nu$ ,  $W$ , and  $\Phi$ . From our solution we see by (2.14) that (4.13a) (or (4.15)) uniquely determines  $\nu$ . However, from (2.15) we see that (4.13b) specifies only a linear combination of  $W$  and  $\Phi'$ , giving one some freedom in how to design a medium with the desired spectral characteristics. In Figure 2.1 two gratings with identical  $\nu$ ,  $\kappa$ , and  $V$  are displayed. The solid curve corresponds to the choice  $\Phi = 0$  (no phase shift in the the refractive index), and the dashed curve corresponds to the choice  $W(Z) = 0$  (no modulation to the DC component of the refractive index).

### 4.3 More general defect gratings

In this section we consider a class of defect gratings which generalizes those studied in the previous section:

$$\kappa(Z) = \sqrt{\omega^2 + n^2 k^2 \tanh^2(kZ)}; \quad (4.17a)$$

$$V(Z) = \frac{\omega n k^2 \operatorname{sech}^2(kZ)}{2(\omega^2 + n^2 k^2 \tanh^2(kZ))}. \quad (4.17b)$$

We shall use this class of defects extensively in numerical simulations. This family of defects can be obtained by specifying an exponentially localized

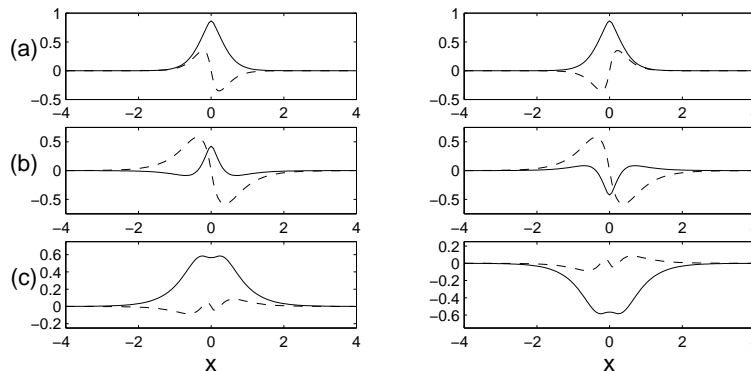


Figure 4.2: The three eigenmodes for the defect (4.17) with  $(\omega, k, n) = (-1, 2, 2)$ . In each plot  $E_+$  is in the left column and  $E_-$  in the right. Solid and dashed lines correspond to real and imaginary parts, respectively.

eigenfunction of (4.5) and then deriving a potential for which this function is a bound state. The calculation is presented in Appendix B. The generalization of the eigenmode (4.11) is

$$\begin{pmatrix} E_+ \\ E_- \end{pmatrix} = \begin{pmatrix} e^{\frac{i}{2} \arctan \frac{nk \tanh(kZ)}{\omega}} \\ e^{-\frac{i}{2} \arctan \frac{nk \tanh(kZ)}{\omega}} \end{pmatrix} e^{-i\omega t} \operatorname{sech}^n(kZ). \quad (4.18)$$

When  $n > 1$  in (4.17), then the linearized equations (4.1) have multiple bound states. For example when  $(\omega, k, n) = (-1, 2, 2)$ , there are three eigenvalues  $\omega_0 = -1$  and  $\omega_{\pm 1} = \pm\sqrt{13}$ . The eigenfunctions are shown in Figure 4.2.

The photonic band gap width is determined by the asymptotic behavior of  $\kappa$  in (4.17a) and is given by  $2\kappa_\infty$ , where

$$\kappa_\infty = \lim_{Z \rightarrow \infty} \kappa(Z) = \sqrt{\omega^2 + n^2 k^2}. \quad (4.19)$$

In our computer simulations (see Section 6) we will set  $k^2 = k_n^2 = C^2/n^2$ , thereby fixing the gap width equal to  $2\sqrt{\omega^2 + C^2}$  and vary the defect width by varying the parameter  $n$ .

The defect  $\kappa(Z)$  varies between the values  $\kappa_0 = |\omega|$  and  $\kappa_\infty = \sqrt{\omega^2 + n^2 k^2}$ . Therefore the “depth”  $\Delta_*$  of the defect is given by

$$\Delta_* = \sqrt{\omega^2 + n^2 k^2} - |\omega|. \quad (4.20)$$

We define the defect width (FWHM) to be given by twice the value of  $Z$  for which  $\kappa(Z) = \frac{1}{2}(\kappa_0 + \kappa_\infty)$ , yielding

$$\text{FWHM} = \frac{2}{k} \tanh^{-1} \left( \frac{\sqrt{2|\omega| \sqrt{\omega^2 + n^2 k^2} + n^2 k^2 - 2\omega^2}}{2nk} \right) \quad (4.21)$$

in the nondimensional setting. Dimensional values for the defect depth and width are provided in Appendix A.

## 5 Nonlinear defect modes

In this section we show that the linear defect modes of Section 4, upon inclusion of nonlinear terms, deform into nonlinear defect modes in a sense to made precise below. We begin by observing that the dimensionless nonlinear coupled mode equations (2.19) can be written in the vector form:

$$(i(\partial_T + \sigma_3 \partial_Z) + \sigma_1 \kappa(Z) + V(Z))E + \Gamma N(E, E^*)E = 0, \quad (5.1)$$

where  $E$  is the two-vector with components  $E_\pm$ ,  $\sigma_1$  and  $\sigma_3$  are displayed in (4.3), and the  $N(E, E^*)$  defines the nonlinear term:

$$N(E, E^*) = \begin{pmatrix} |E_+|^2 + 2|E_-|^2 & 0 \\ 0 & |E_-|^2 + 2|E_+|^2 \end{pmatrix} \quad (5.2)$$

**Bifurcation of nonlinear defect modes** We assume that all eigenvalues of the linearized problem (4.1) are simple, which has been found numerically for the family of defects investigated. Let  $E_0 = e^{-i\omega_0 T} \mathcal{E}_0(Z)$  denote a linear defect mode. That is,  $\mathcal{E}_0(Z)$  is a spatially localized solution of the equation

$$(\omega_0 + i\sigma_3 \partial_Z + \sigma_1 \kappa(Z) + V(Z))E = 0. \quad (5.3)$$

We seek to construct *nonlinear* bound states of (5.1) of the form:

$$E(Z, T) = e^{-i\omega T} \mathcal{E}(Z), \quad (5.4)$$

where

$$\begin{aligned} \mathcal{E}(Z) &= \alpha (E_0(Z) + |\alpha|^2 E_1(Z) + \mathcal{O}(|\alpha|^4)) \\ \omega &= \omega_0 + \omega_1 |\alpha|^2 + \mathcal{O}(|\alpha|^4) \end{aligned} \quad (5.5)$$

and  $\alpha$  is a small parameter. Since for any  $\omega$ ,  $\mathcal{E}(Z) \equiv 0$  is a solution of (5.3), solutions of the form (5.5) are said to *bifurcate* from the trivial solution at  $\omega = \omega_0$ .

Substitution of (5.5) into (5.1) yields a hierarchy of inhomogeneous linear equations beginning with:

$$\mathcal{O}(1) : \mathcal{L}_0 E_0 = 0 \quad (5.6a)$$

$$\mathcal{O}(|\alpha|^2) : \mathcal{L}_0 E_1 = -\omega_1 E_0 - \Gamma N(E_0, E_0^*)E_0 \quad (5.6b)$$

where

$$\mathcal{L}_0 = \omega_0 + i\sigma_3\partial_Z + \sigma_1\kappa + V. \quad (5.7)$$

is a linear self-adjoint operator. The first equation in (5.6) holds if  $E_0 = \mathcal{E}_0$ , any linear defect mode,  $\mathcal{E}_0$  of frequency  $\omega_0$ . The eigenvalue  $\omega_0$  is necessarily of multiplicity one. The second equation in (5.6) is solvable for a localized correction term,  $\mathcal{E}_1$  if and only if the right hand side of the equation is orthogonal to the null space (zero energy subspace) of  $\mathcal{L}_0$ . Imposing this orthogonality condition yields the following equation which determines the value of  $\omega_1$ :

$$\langle \mathcal{E}_0 | \omega_1 \mathcal{E}_0 + \Gamma N(\mathcal{E}_0, \mathcal{E}_0^*)\mathcal{E}_0 \rangle = 0. \quad (5.8)$$

We obtain from (5.8):

$$\omega_1 = -\Gamma \frac{\langle \mathcal{E}_0 | N(\mathcal{E}_0, \mathcal{E}_0^*)\mathcal{E}_0 \rangle}{\langle \mathcal{E}_0 | \mathcal{E}_0 \rangle} \quad (5.9)$$

It follows that the nonlinear defect mode bifurcating from the linear defect mode of frequency  $\omega_0$  is:

$$E(Z, T) = e^{-i\omega T} \alpha (\mathcal{E}_0(Z) + |\alpha|^2 \mathcal{E}_1(Z) + \mathcal{O}(|\alpha|^4)) \quad (5.10)$$

$$\omega = \omega_0 + |\alpha|^2 \omega_1 + \mathcal{O}(|\alpha|^4) \quad (5.11)$$

We shall refer to the nonlinear defect mode bifurcating from  $\omega = \omega_0$  as an  $\omega_0$ -nonlinear defect mode. Since  $\Gamma > 0$  (see Section 2), the bifurcating states have frequencies below  $\omega_0$ .

A rigorous proof of the existence of bifurcating nonlinear defect modes and the validity of this expansion can be given in a manner analogous to that carried out in the context of the nonlinear Schrödinger equation [20].



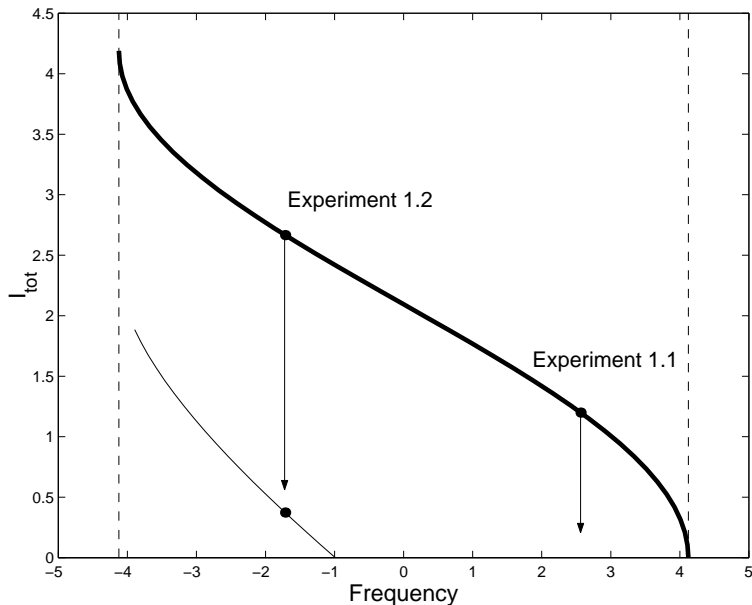


Figure 5.1: Intensity vs. frequency for the gap soliton (bold) and a nonlinear defect mode with parameters  $(\omega_0, k) = (-1, 4)$ .

Numerically we are able to find nonlinear defect modes for values of  $\alpha$  much larger than zero. A plot of the intensity vs. frequency for one such family of defect modes is shown in Figure 5.1. For the spatially homogeneous case, gap solitons are seen to bifurcate from the zero state at the right endpoint of the continuous spectrum,  $\omega = \kappa_\infty = \sqrt{17}$ . For the given defect, a branch of nonlinear defect modes bifurcates from the zero state at  $\omega = \omega_0 = -1$ . The nonlinear defect mode and its frequency become difficult to compute as the frequency  $\omega$  of the nonlinear mode approaches an endpoint of the continuous spectrum, because the exponential decay rate decreases and larger spatial intervals must be used in order to compute the exponential tail.

## 6 Computer simulations of a gap soliton incident on a defect

In Section 3 we discussed gap solitons, the fundamental nonlinear bound state of propagation in a uniform periodic structure. In Section 4 we then

considered the linear modes of a periodic structure with a defect and, in Section 5, the nonlinear defect modes which bifurcate from these linear defect modes. In this section we study by computer simulation the dynamics of a gap soliton incident on a defect.

In Section 2, we derived a nondimensional form of the coupled mode equations with nondimensional parameters  $\kappa(Z)$ ,  $V(Z)$ , and  $\Gamma$  given by (2.20). By an additional rescaling of the nondimensional variables  $Z$ ,  $T$ , and  $E_{\pm}$ , we may redefine the equations so that  $\Gamma = 1$  and  $\kappa_{\infty}$  takes the form given in equation (4.19). In other words,  $\kappa_{\infty}$  and  $\Gamma$  can be set arbitrarily and the results can always be mapped to a physical system.

Simulations indicate complex interactions between the incident gap soliton (Section 3) and the modes of defect (Sections 4 and 5). *An understanding of the dynamics and the potential for trapping requires an understanding of the energy exchange between the gap soliton mode and nonlinear defect modes.* Our numerical simulations give strong support to the following hypothesis suggested by the notions of resonant energy transfer and energy conservation.

**Hypothesis.** *Consider a gap soliton incident on a defect with sufficiently low incident velocity. The gap soliton will transfer its energy to a nonlinear defect mode, and thereby be trapped, if there exists a nonlinear defect mode of the same frequency **and** lower total intensity ( $L^2$  norm). Otherwise, the gap soliton energy will be reflected and/or transmitted.*

We now describe our numerical experiments. The defects described in Section 4 are members of a 3-parameter  $(\omega_0, k, n)$  family and the gap solitons are described by two parameters  $(v, \delta)$ . While it is not possible to investigate all of the soliton-defect interactions in this 5-dimensional space, we have performed a large number of simulations, and were able to draw some general conclusions. We concentrate on gap solitons of comparable width and amplitude to the defects, so that linear and nonlinear interactions are likely to be strong and balanced. Physical experiments have so far produced pulses with relatively large values for  $v$  and small values for  $\delta$ , so we make some attempt to trap gap solitons in this parameter regime. Dimensional equivalents for most of the nondimensional experiments are given in Appendix A. Intensities range from 130 to 1800 GW/cm<sup>2</sup>, pulse widths are between 1.3 and 4.4 mm, and defect widths are between 1.6 and 4.7 mm (FWHM). Note that in this section, the frequency of the linear defect mode is given by  $\omega_0$ , while  $\omega = \kappa_{\infty} \cos \delta$  is the frequency of a stationary gap soliton.

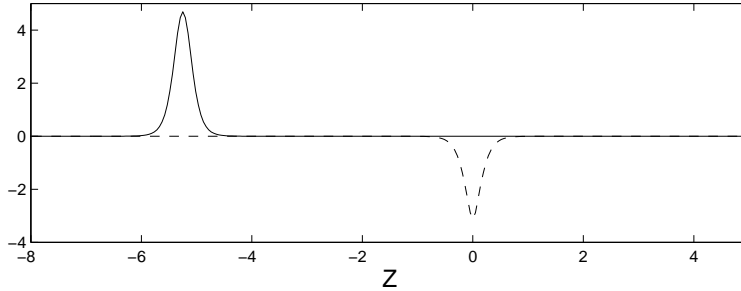


Figure 6.1: (Experiment 1.1) The initial value of  $|E_+|^2 + |E_-|^2$  (solid line), which gives the approximate strength of the nonlinear forcing, and of the defect  $\kappa(Z) - \kappa_\infty$  (dashed), which gives the forcing due to the defect.

## 6.1 Experiment 1: Gap soliton incident on a dark soliton defect gratings

We first consider the simplest case of pulses interacting with the dark soliton defect gratings defined in (4.13). We consider a defect with  $k = 4$  and  $\omega_0 = -1$ . This defect supports a single nonlinear bound state. The key insight into predicting whether the gap soliton interacts strongly with the defect is found by examining Figure 5.1. A gap soliton with frequency  $\omega = \kappa_\infty \cos \delta$  will interact most strongly with the defect if a nonlinear defect mode exists with the same frequency and equal or less total intensity. If it does, then it is possible for the gap soliton to resonantly transfer its energy to the defect mode. The relevant mechanism seems not to be the slowing of the soliton, rather this transfer of energy. Note from the figure that for  $\omega < -1$  ( $\delta > 1.82$ ) such modes exist, and for larger  $\omega$  they do not. Of course, the gap soliton frequency-intensity curve given in the figure applies only in the case  $v = 0$ , but it is useful for making predictions for small  $v$ .

**Experiment 1.1** (Reflection/Transmission) With the defect parameters set, we then investigate a two parameter family of gap solitons indexed by the velocity  $v$  and the detuning  $\delta$ . Our first experiment is for detuning  $\delta = 0.9$ . Via inspection, the pulse is of comparable depth and width to the defect, so seems an ideal candidate for capture, see Figure 6.1. However, the central frequency of this gap soliton at small velocities is  $\kappa_\infty \cos \delta \approx 2.56 > \omega_0 = -1$ , so we do not expect the defect mode to be strongly forced by the gap soliton.

Indeed, although we observe a slowing, and therefore delay, of the gap

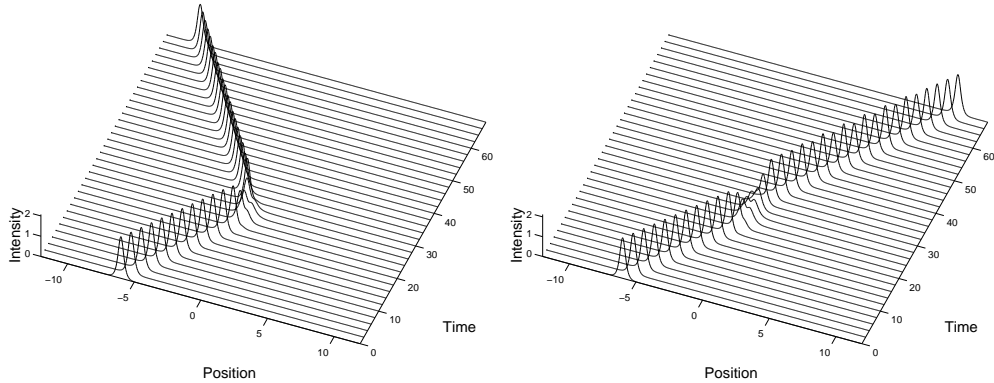


Figure 6.2: (Experiment 1.1) At left, a gap soliton with  $v = .2565$  is reflected by a defect at  $Z = 0$ . At right, a slightly faster gap soliton with  $v = .257$  is transmitted.

soliton we do not find significant excitation of the defect mode or trapping. We find that below a critical velocity  $v \approx 0.257$ , all gap solitons are reflected, and above this speed they are transmitted. The closer the incoming pulse comes to this incoming velocity, the longer it remains in the neighborhood of the defect before being ejected and the velocity of the outgoing pulse is approximately that of the incoming pulse.

In Figure 6.2, we show the evolution of two gap solitons incident on the defect, both very close to the critical velocity, showing clearly the effects discussed above.

Interestingly, the gap soliton *slows down* when it nears the defect (Figure 6.2 for times between 20 and 30). This is somewhat unexpected; as the defect supports a bound state, one intuitively expects the soliton center of mass to move as a “classical particle in a potential well”. Instead the soliton behaves more like a classical particle encountering a potential barrier. Broderick and de Sterke conjecture that if a defect supports bound states, then a particle approaching it should “see” a potential well, and if it supports no bound state, then an approaching gap soliton should see a barrier [5]. Our numerical simulations and theory, based on energy conservation and resonant energy transfer illustrate that the situation is more complex. Indeed, both the “potential well like” and “potential barrier like” behavior are possible for a defect that supports bound states.

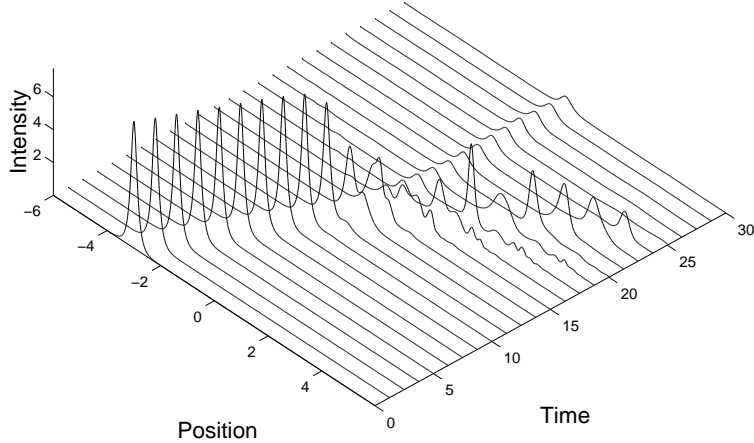


Figure 6.3: (Experiment 1.2) With  $\delta = 2$ , a defect mode of significant intensity remains behind after the soliton passes through. (Due to the absorbing boundary conditions used in the simulations, the gap soliton dissipates as it approaches the edge of the computational domain)

The reflection of these gap solitons is well-explained by Figure 5.1. To test our hypothesis, we post-process the numerical experiment as follows. At each time step, we compute the projection of the solution onto the linear defect mode of this defect, and find that when the gap soliton is directly over the defect, the projection onto the bound state accounts for only 6% of the total  $L^2$  norm of the solution, and after the soliton escapes, the projection accounts for less than 0.2% of the solution. As there is no resonant exchange of energy between soliton and defect mode, the soliton escapes.

**Experiment 1.2** (Trapping for larger intensities) Figure 5.1 suggests that gap solitons with larger values of the detuning  $\delta$ , may interact more strongly with the defect. We therefore run the experiment again with  $\delta = 2$  (frequency  $\omega = -1.72$ ) below  $\omega_0$ , and  $v = 0.2$  the results of which are shown in Figure 6.3. When the soliton encounters the defect, it seems to split into three parts: a transmitted soliton, a trapped mode, and radiation. The mode that remains at the defect has only about 16% of the total intensity of the

incoming gap soliton. Remarkably, at the end of the computation, the captured state's frequency is approximately  $\omega = -1.7$  and the solution's total intensity is such that the trapped energy is described by a point very close to the nonlinear bound state curve of Figure 5.1. This supports the first part of our hypothesis. For small values of  $v$ , the amplitude and frequency of the trapped state do not seem to depend on  $v$ . Above a certain larger velocity, significantly less energy is trapped by the defect, suggesting that the hypothesis needs refinement for large velocities.

**Experiment 1.3** (Refining these results) Clearly, this computation shows that we can use a defect to trap a significant portion of the electromagnetic energy in a gap soliton. However to this point, the gap solitons we have captured have had very high intensities, and further, only a small amount of the solitons energy is trapped by the defect. It is of interest to trap lower intensity pulses, and it would be preferable if a larger fraction of the soliton's energy were trapped by the defect. The nonlinear defect modes always bifurcate to the left from the linear defect mode frequency for increasing intensity. Consider the defect defined by (4.13) with  $k = 4$  as before, but now letting  $\omega_0 = 1$ . This leaves  $\kappa(Z)$  unchanged, while changing the sign of  $V$ . This moves the base of the nonlinear bound state curve to  $\omega_0 = +1$ , so that the intensity–frequency curves for the nonlinear defect mode and the gap solitons are significantly closer together; see Figure 6.4. If we examine the interaction of  $\delta = \pi/2$  ( $\omega = 0$ ) gap solitons with each of these defects, the bifurcation diagrams anticipate that the  $\omega_0 = 1$  defect will capture a lot of energy from the pulse, while the  $\omega_0 = -1$  defect will reflect or transmit the pulse, depending on its incoming velocity. Numerical experiments show this to be the case.

We can further improve trapping using the dark-soliton family of defects by increasing the ratio  $\omega_0/\kappa_\infty$ . The gap edge is at  $\kappa_\infty = \sqrt{\omega_0^2 + k^2}$ , while the defect mode curve starts at  $\omega_0$  and goes left with increasing intensity. The problem with this approach is that as  $\omega_0 \rightarrow \kappa_\infty$ , the the width of the gap increases without bound, while its depth goes to zero.

## 6.2 Experiment 2: Gap soliton incident on grating defects supporting multiple bound states

We now show how to use the generalized dark soliton defects of Section 4.3 to more efficiently capture solitons. As pointed out in the paragraph follow-

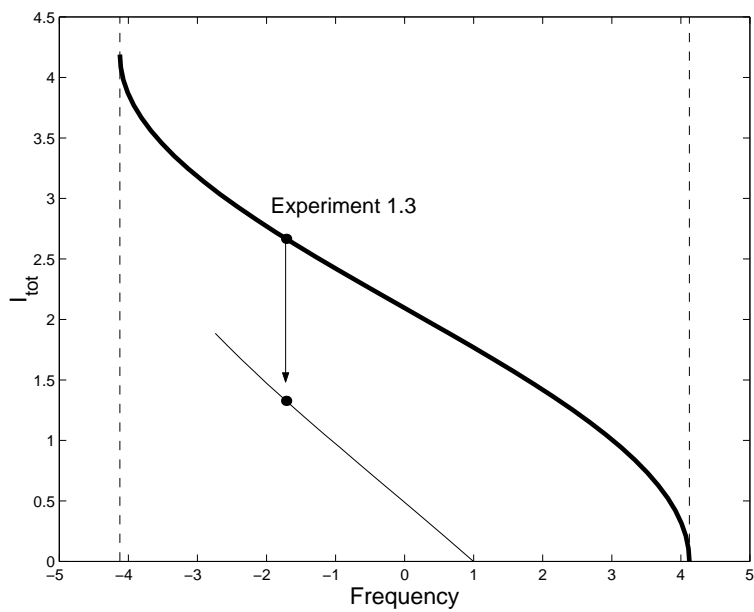


Figure 6.4: Intensity vs. frequency for the gap soliton (bold) and a nonlinear mode for defect with parameters  $(\omega_0, k) = (1, 4)$ . Although the defect is the same as that used in Figure 5.1 excepting a sign in the definition of  $V(Z)$ , the defect mode curve is further to the right and closer to the gap soliton curve, predicting greatly improved trapping.

ing (4.19), we can use defects given by (4.17) to fix the spectral gap and study the interaction of gap solitons with defects of different widths. We next study gap solitons incident on a grating of this form with  $(\omega_0, k, n) = (-1, 2, 2)$ . This defect is twice the width of the dark soliton defect grating of Section 6.1, but has the same limiting profile far from the defect region. From, Appendix B, the defect supports three linear bound states, with ground state frequency  $\omega_0 = -1$  and excited states  $\omega_{\pm 1} = \pm\sqrt{13}$ . Branches of nonlinear defect modes bifurcate from each of these linear modes. Figure 6.5 is the analog of Figure 5.1 for this defect. To the left of the indicated frequency  $\omega_*$ , the  $\omega_{+1}$ -nonlinear defect mode has greater intensity than the gap soliton. The frequencies  $\omega_{-1}$ ,  $\omega_0$ ,  $\omega_*$ , and  $\omega_{+1}$  divide the band gap into 5 regions. In the regions  $-\kappa_\infty < \omega < \omega_0$  and  $\omega_* < \omega < \omega_{+1}$  we expect by the same mechanisms as in Experiment 1.2 to find trapping of energy, while in the regions  $\omega_0 < \omega < \omega_*$  and  $\omega_{+1} < \omega < \kappa_\infty$ , we do not expect trapping. In the segment  $-\kappa_\infty < \omega < \omega_{-1}$ , we expect complex behavior because two trapped nonlinear modes coexist. We expect the most efficient capture for solitons with frequency slightly greater than  $\omega_*$ , for which a nonlinear bound state exists of slightly lower total intensity than the incoming pulse.

**Experiment 2.1:** (The trapping region  $\omega_* < \omega < \omega_{+1}$ )

**(2.1a)** We first examine gap solitons with  $\delta = 0.9$ , ( $\omega \approx 2.6$ ) which lie just to the right of  $\omega_*$  in Figure 6.5. Trapping here is relatively efficient, because a soliton can transfer almost all its amplitude to the nonlinear defect mode of the same frequency and slightly lower intensity. We find trapping for gap solitons slower than a critical velocity of about  $v_c = 0.102$ . In Figure 6.6, we show the evolution of a gap soliton, initially propagating to the right, which gets trapped. In Figure 6.7, we show the position vs. time plot for a gap soliton that gets trapped and one that escapes. In both cases, the gap soliton speeds up on reaching the defect, consistent with the defect acting as a potential well. Figure 6.8, shows the output soliton velocity as a function of the soliton input velocity in a region near the critical velocity. The figure indicates a sharp transition at a critical velocity from gap solitons which are trapped to gap solitons which propagate through.

Although the NLCME system (2.19) conserves  $I_{\text{tot}}$ , radiation may carry some energy away from the defect. The computations are performed on a finite domain with absorbing boundary conditions, so that radiation losses



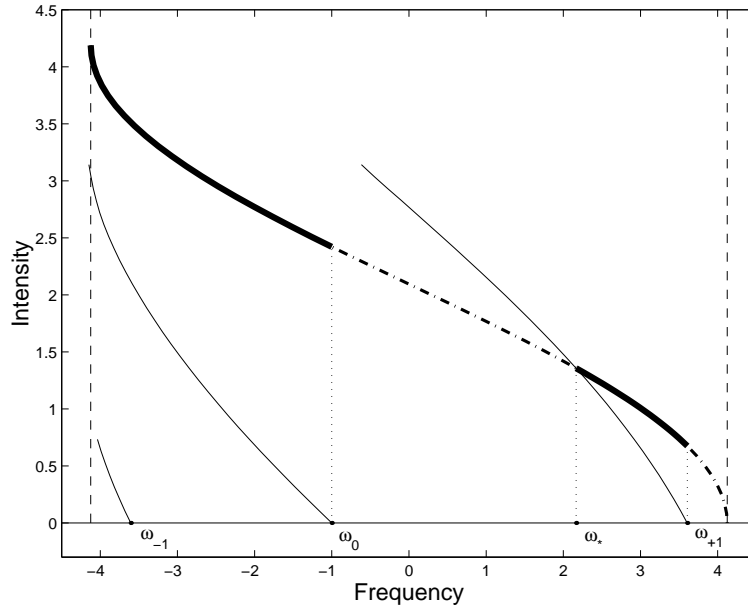


Figure 6.5: Intensity vs. frequency for the gap soliton (bold) and the three nonlinear mode for defect with parameters  $(\omega_0, k, n) = (-1, 2, 2)$ . Trapping is possible for frequencies on the thickened section of the gap soliton curve.

Figure 6.6: (Experiment 2.1a) A typical picture of the capture of a gap soliton by a defect centered at  $Z = 0$ .

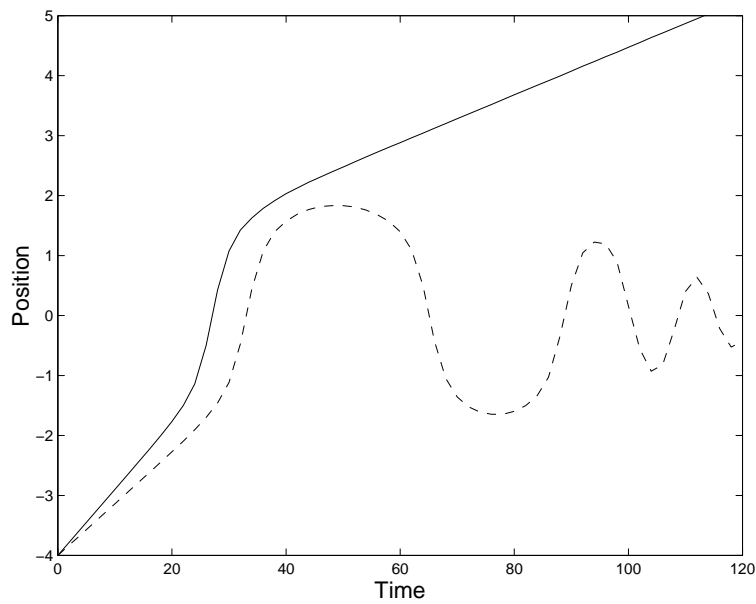


Figure 6.7: (Experiment 2.1a) The position vs. time of an escaping and a captured gap soliton. Note that the instantaneous velocity increases when the gap soliton is in the defect region ( $Z$  near zero).  $\delta = 0.9$ ,  $v$  near  $v_c \approx 0.103$ , the potential as described in subsection 6.2.

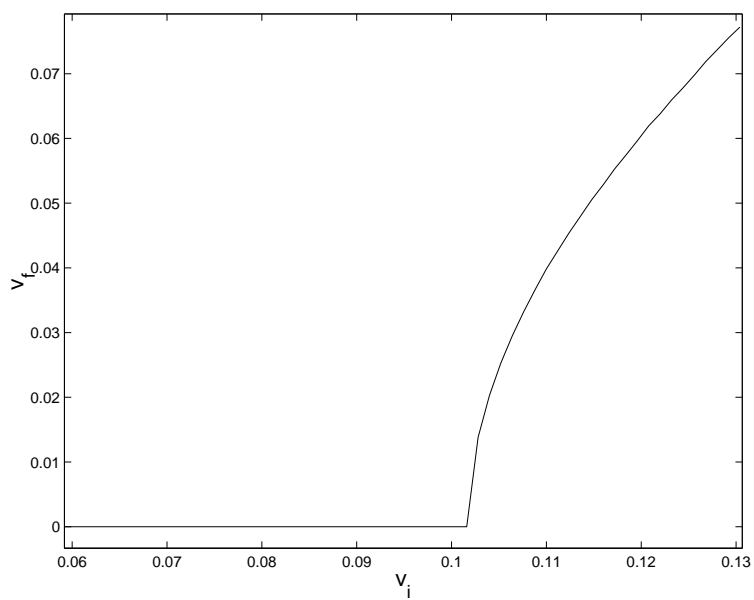


Figure 6.8: (Experiment 2.1a) Initial velocity ( $v_i$ ) vs. final velocity ( $v_f$ ) of gap soliton, parameters as in 6.7 with variable  $v$ .

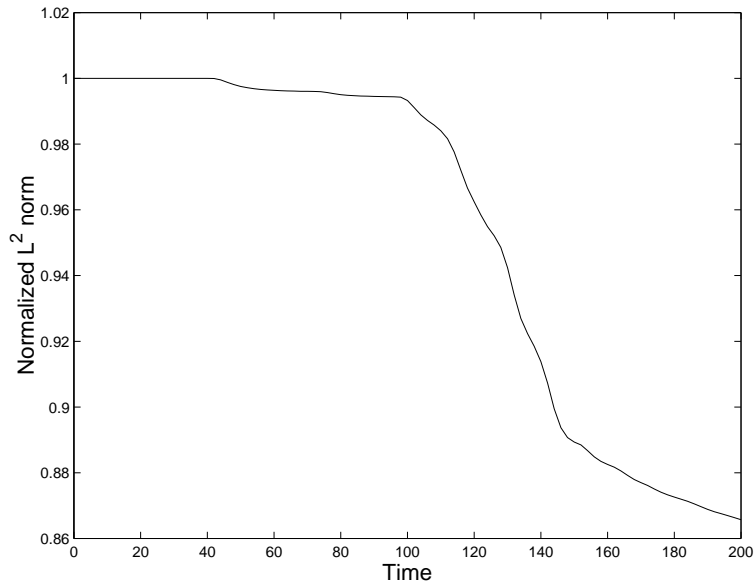


Figure 6.9: Decay of the local  $L^2$  norm (normalized) for Experiment 2.1a.

can be measured by monitoring the local  $L^2$  norm, *i.e.*

$$\text{Local } L^2 \text{ norm} = \left( \int_D |E_+|^2 + |E_-|^2 dZ \right)^{\frac{1}{2}},$$

where  $D$  is a bounded region containing the defect; see Figure 6.9. By time  $t = 120$ , the energy has been transferred from the soliton to the nonlinear defect mode, but the system continues losing energy to radiation at a constant rate for the length of the simulation.

**(2.1b)** For the slightly a smaller value of  $\delta = 0.6$ , the distance between the gap soliton curve and the nearby defect-mode curve in Figure 6.5 is increased. Some of the energy is deposited in a defect mode, while the remaining energy appears to propagate as a diminished gap soliton plus small radiation; see Figure 6.10.

There is not space to report in detail on all of the behaviors found in the numerical simulations for this defect. As expected, gap solitons with frequency  $\omega < \omega_0$  are trapped in a similar manner to those in Experiment 1.2. When  $\omega < \omega_{-1}$ , then all three nonlinear modes are excited by the gap soliton. More unexpectedly, in the region  $\omega_0 < \omega < \omega_*$ , the gap soliton, while never

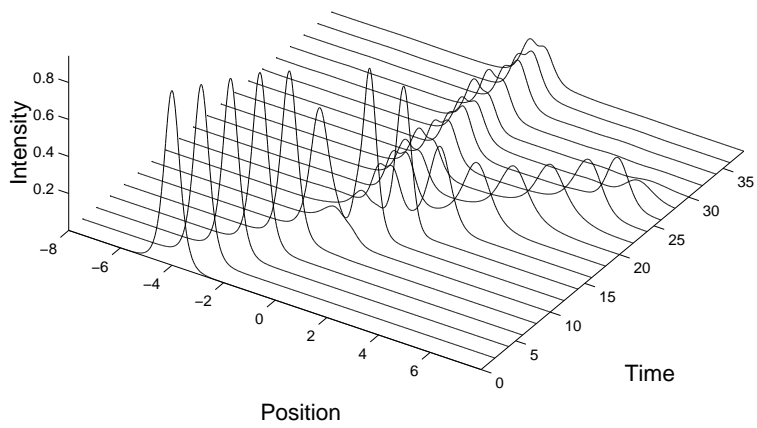


Figure 6.10: (Experiment 2.1b) Partial capture; an incident gap soliton results in part of its energy captured in the defect and part transmitted as a lower energy gap soliton

Figure 6.11: (Experiment 2.2a) Capture of a gap soliton with  $\delta = 0.45$  by a wide well.

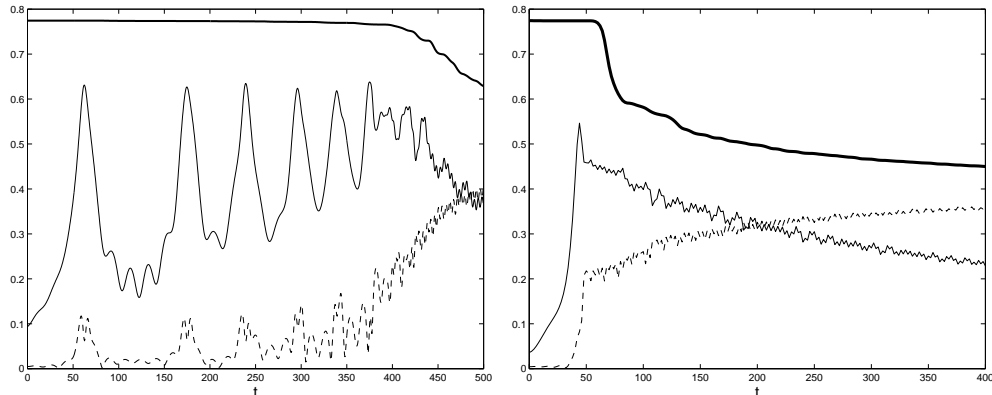


Figure 6.12: Local  $L^2$  norm of the solution (bold), the projection onto the  $\omega_{+2}$  eigenmode (solid) and the  $\omega_{+1}$  mode (dashed) for Experiment 2.2a (left) and 2.2b (right).

captured, is never reflected either. In this frequency range, for every initial velocity as low as  $v = .0006$ , the soliton is transmitted after slowing down slightly when encountering the defect.

**Experiment 2.2:** (Wider defects)

**(2.2a):** By widening the defect, we may place more eigenvalues closer to the edges of the band gap which might then be used to trap gap solitons with even smaller  $\delta$ . Using a defect with parameters  $(\omega_0, k, n) = (-1, 1.6, 2.5)$  (keeping  $\kappa_\infty = \sqrt{17}$  as in previous sections), which has 5 eigenvalues  $\omega_0 = -1$ ,  $\omega_{\pm 1} = \pm\sqrt{281}/5$ ,  $\omega_{\pm 2} = \pm\sqrt{409}/5$ , we captured a soliton with  $\delta = 0.45$ , although with the velocity significantly reduced to about  $v = 0.025$ . We found that the defect with  $k = n = 2$  described in Experiment 2.1 reflects this gap soliton, as its central frequency is to the right of the defect mode curve in Figure 6.5. The dynamics of the soliton captured by the present defect is shown in Figure 6.11. At about  $t = 400$  the trapped mode begins to lose intensity to radiation, as is more clearly seen in Figure 6.12a; note the decay of the local  $L^2$  norm beginning around  $t = 400$ .

Also shown in Figure 6.12 are the numerical projection onto the linear eigenfunctions belonging to  $\omega_{+2}$  and  $\omega_{+1}$ . At capture time ( $t \approx 60$ ), the solution is dominated by the  $\omega_{+2}$  mode. At longer times, however, this trapped mode is not persistent and the energy is transferred from  $\omega_{+2}$  to  $\omega_{+1}$ , with a lot of energy lost to radiation and very little in the other three eigenmodes.

**(2.2b):** The effect of defect width can be further explored. In the next experiment, we widen the defect further, by choosing parameters  $k = 4/3$ ,  $n = 3$  in (4.17a), and choose the same gap soliton parameters as in the above paragraph. The defect is slightly wider than in Experiment 2.2a, though it still supports five linear bound states, with eigenvalues slightly smaller than in the previous paragraph:  $\omega_0 = -1$ ,  $\omega_{\pm 1} \pm \sqrt{89}/3$ ,  $\omega_{\pm 2} = \pm \sqrt{137}/3$ . In this case, the trapping is significantly less effective. A much smaller bound state is trapped. As in the previous experiment, most of the energy is localized in the modes belonging to  $\omega_{+1}$  and  $\omega_{+2}$ , although, as seen in Figure 6.12, the  $\omega_{+1}$ -mode begins growing sooner.

### 6.3 Experiment 3: Defect arrays

Figure 6.8 shows that gap solitons which are not trapped by a defect may be severely slowed. This suggests that an array of defects of the type discussed above can be used to successively slow and then trap a gap soliton. Using a pair of defects, we have been able to trap a gap soliton whose initial velocity was 50% higher than the critical velocity found in Experiment 2.1. We construct defect arrays  $\kappa_2(Z)$  and  $V_2(Z)$  by forming  $\kappa(Z)$  and  $V(Z)$  of subsection 6.2 and then letting  $\kappa_2 = \kappa(Z - Z_1) + \kappa(Z - Z_2) - \kappa_\infty$  and  $V_2(Z) = V(Z - Z_1) + V(Z - Z_2)$ . Such gratings with  $Z_1 = -3$  and  $Z_2 = 3$  are shown in Figure 6.13. In Figure 6.14 we show the position vs. time for gap soliton with  $\delta = .9$ ,  $v = .15$ , which is slowed by the first well and then captured by the second.

### 6.4 Experiment 4: Side barriers

In the previous sections, we captured light by transferring energy from a gap soliton to a nonlinear defect mode. In this section, by contrast, we trap a moving soliton between two obstacles. In Experiment 1.1, solitons with frequency to the right of the ground state frequency were slowed but not trapped upon encountering the defect. We modify the defect by adding a

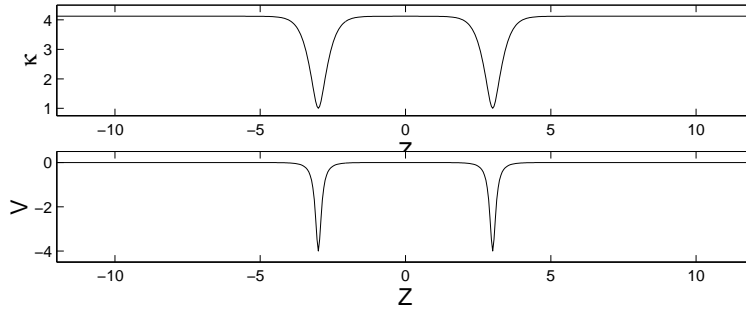


Figure 6.13: (Experiment 3)  $\kappa(Z)$  and  $V(Z)$  for an array of two defects.

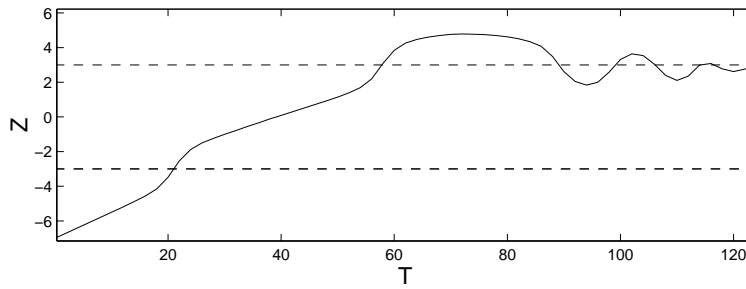


Figure 6.14: (Experiment 3) Position vs. time for a gap soliton incident on an array of defects. Defect positions given by dashed lines.



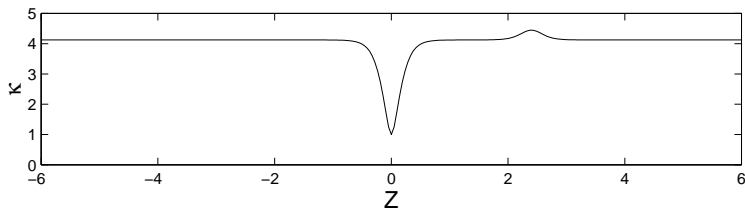


Figure 6.15: (Experiment 4) The modified defect described in 6.4.

bump or “potential barrier” away from the main defect; see Figure 6.15. This configuration of defects traps the gap soliton in a novel way. Instead of a bound state forming near the minimum of  $\kappa(Z)$ , the gap soliton bounces back and forth between the old “well” and the new “bump” that has been added. Further, it captures a pulse with an incident speed of  $v = .3$ , about 3 times the critical velocity for the generalized dark soliton grating described in Experiment 2.1. In addition, the rate of energy loss for gap solitons captured by this defect is significantly reduced. Figure 6.16 shows the rate of energy loss for gap solitons with  $\delta = .9$  and velocities  $v = .2625$  and  $v = .3$ . It shows that, although it can capture gap solitons moving this fast, as the speed increases, the efficiency of the capture decreases.

## 7 Nonlinear damping effects

As we have shown in the preceding section, the gap solitons for which we have been able to find interesting capture behavior have all had large values of  $\delta$ . (So large, in fact, that perhaps silica fibers would not be able to support pulses of that intensity.) One potential way to make use of our theoretical solutions would be to use fibers with larger nonlinear refractive index  $n_2$ . We see by equation (A.9) that the intensity of a gap soliton, for fixed  $v$  and  $\delta$ , is inversely proportional to  $n_2$ . *Chalcogenide* fibers, for which  $n_2$  is as much as 500 times larger than in silica fibers, are a promising material in which one could potentially observe the phenomena discussed above at lower intensities. Unfortunately, in chalcogenide fibers, the imaginary part of  $n_2$  is also significantly larger, corresponding to nonlinear damping arising from *multiphoton absorption*. By choosing a chalcogenide glass composition that minimizes both two photon and three photon absorption, one can achieve

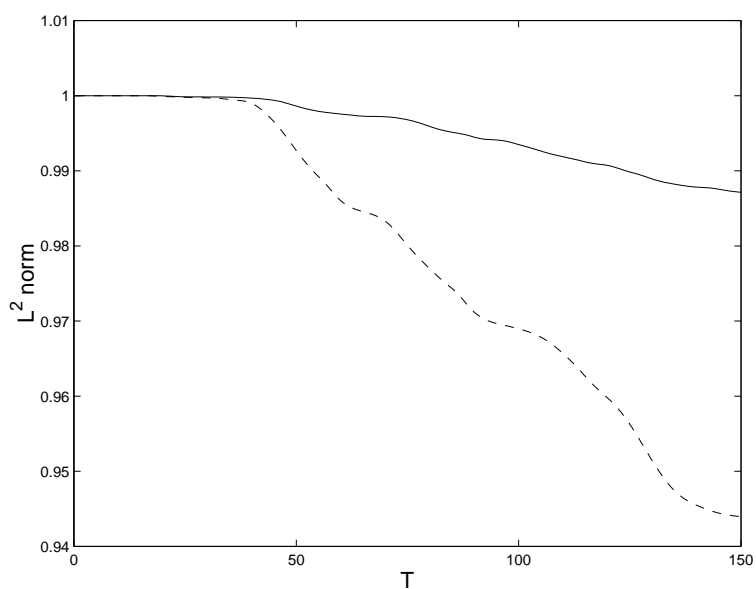


Figure 6.16: (Experiment 4) Local  $L^2$  norm as a function of time for gap soliton with  $v = .2625$  (solid) and  $v = .3$  (dashed).

an  $n_2$  nearly 500 times silica while suffering a multiphoton loss of a few percent at intensities required for a nonlinear phase shift of  $\pi$ .

In terms of the coupled mode equations, a complex cubic refractive index gives rise to a complex coefficient  $\Gamma$ . Due to the symmetries of the NLCME and the gap soliton, the magnitude of  $\Gamma$  is unimportant, as gap solitons have intensity that scales as  $1/\Gamma$ . What will be important is the ratio  $\Gamma_i/\Gamma_r$ . In this case we are more interested in simply simulating the propagation of pulses which at  $t = 0$  correspond to gap solitons. The strength of the damping is proportional to  $I_{\max}$ , or  $\sin^2 \frac{\delta}{2}$ . Therefore as we decrease  $\delta$  the effect of the nonlinear damping should be decreased. However, if decreasing  $\delta$  requires a decrease in the gap soliton velocity  $v$  for trapping, so that pulses will have more time to decay as they propagate before reaching the defect. We ran one set of experiments with  $\Gamma_i/\Gamma_r = 0.1, 0.01, \text{ and } 0.001$ , with  $v = 0.2$  and  $\delta = 0.9$ , and with the generalized dark soliton grating with  $\omega_0 = -1, k = 2$ , and  $n = 2$ . Without nonlinear damping, the defect will not capture these solitons. The soliton was initialized 5 units to the left of the defect center. With the damping ratio .1, the gap soliton is mainly damped before it even reaches the defect. With ratio .01, the pulse loses just enough energy that much of it is captured upon reaching the defect. With the ratio .001, the gap soliton propagates through the defect untrapped.

## 8 Summary and discussion

Gap solitons are localized nonlinear bound states which propagate in periodic structures. We have investigated by analytical and numerical methods the possibility of capture of gap solitons by the introduction of appropriately designed defects, spatially localized deviations from exact periodicity.

We first displayed interesting classes of defects which support trapped defect modes of the linear coupled mode equations. We then showed that these linear defect modes, deform into *nonlinear defect modes* of the nonlinear coupled mode equations. Bifurcation diagrams of total intensity ( $I_{\text{tot}}$ ) versus frequency suggest the following hypothesis: for sufficiently low velocities, a gap soliton incident on a defect will transfer its energy to a nonlinear defect mode localized at the defect provided there is one of the same frequency (resonance) and lesser total intensity (energetically accessible). This hypothesis is supported by an extensive series of numerical investigations. An understanding of the dependence of the critical velocity requires further

investigation.

We have studied the interaction of gap solitons with defects which support one or multiple linear (and therefore nonlinear) defect modes. In Section 6.2 we show how secondary defect modes can be used to trap energy from lower-amplitude gap solitons, which correspond more closely to the regime accessed thus far in physical experiments. However, in contrast to trapping by a defect mode with a single defect, when gap soliton energy is transferred to the modes of a multimode defect, the dynamics of the localized energy is quite complicated.

We believe that a finite-dimensional model incorporating both soliton and defect mode degrees of freedom could be very useful in understanding the capture problem. In these models the soliton is modeled by several parameters (*e.g.*, position, width, phase) and the defect mode by its "amplitude". A system of ordinary differential equations approximating the dynamics of a soliton interacting with a defect can be obtained from an *effective Lagrangian*, which is a function of these collective variables. Broderick and de Sterke [5] have studied such a model which does not take into account degrees of freedom available in the defect modes. Their model displays some of the observed behaviors but, as we have seen, the mechanism of resonant energy transfer must be included to provide a full explanation.

Similar finite-dimensional models have been studied in [10, 11, 12] for the sine-Gordon,  $\phi^4$  and nonlinear Schrödinger equations. Comparison of models for the trapping of sine-Gordon kinks with and without the defect-mode degrees of freedom [17, 11] demonstrates the necessity of allowing the additional modes of oscillation. We have applied tools of dynamical systems theory to similar reduced models for soliton like structures of the sine-Gordon equation [14] and NLS [13]. These studies give insight into the nature of the set of states incident on the defect resulting in transmission without capture, capture, and capture for all time. Closer qualitative agreement with the full dynamics is obtained by inclusion of a damping term, reflecting the coupling to radiation modes.

## A Calculation of gap soliton characteristics

In this appendix, we derive dimensional values of  $\kappa_\infty$  and  $\tilde{\Gamma}$  in equations (2.14) and (2.16). We use these quantities to estimate the physical parameter values corresponding to the simulations performed in Section 6.

## A.1 Dimensional values of $\tilde{\kappa}_\infty$ and $\tilde{\Gamma}$

It is common to work with the cubic refractive index [2, p.40, 582],  $n_2$  (also denoted  $n_2^I$ ):

$$n_2 = 3\chi^{(3)}/4\epsilon_0 c \bar{n}^2, \quad (\text{A.1})$$

quoted in units of  $\text{m}^2/\text{W}$ . This gives

$$\tilde{\Gamma} = \frac{4\pi\epsilon_0 c \bar{n} n_2}{\lambda_B}. \quad (\text{A.2})$$

We list the parameters needed, as obtained from Eggleton, *et. al.* [9] and from standard sources:

$$\begin{aligned} \lambda_B &= 1053 \text{ nm}; \\ \bar{n} &= 1.45; \\ \Delta n &= 3 \times 10^{-4}; \\ n_2 &= 2.3 \times 10^{-20} \text{ m}^2/\text{W}; \\ c &= 2.98 \times 10^8 \text{ m/s}; \\ \epsilon_0 &= 8.85 \times 10^{-12} \text{ C/Nm}^2. \end{aligned} \quad (\text{A.3})$$

Then the wavenumber in the medium is given by

$$k_B = 2\pi \frac{\bar{n}}{\lambda_B} = 8.7 \times 10^6 \text{ m}^{-1}, \quad (\text{A.4})$$

and  $\tilde{\kappa}_\infty$  (see (2.14)) and  $\tilde{\Gamma}$  by

$$\tilde{\kappa}_\infty = 900 \text{ m}^{-1}, \text{ and} \quad (\text{A.5})$$

$$\tilde{\Gamma} = 1.06 \times 10^{-15} \frac{\text{C}^2}{\text{N}^2\text{m}}. \quad (\text{A.6})$$

## A.2 Converting from nondimensional to dimensional form

Inverting the nondimensionalization relations (2.20), the dimensional length, time and electric field scales can be obtained from the following relationship

$$\mathcal{Z} = \frac{\kappa_\infty}{\tilde{\kappa}_\infty} = \frac{\kappa_\infty \lambda_B}{\pi \Delta n}, \quad \mathcal{T} = \frac{\kappa_\infty \lambda_B \bar{n}}{\pi \Delta n c} \quad (\text{A.7a})$$

$$\mathcal{E}^2 = \frac{\Gamma \tilde{\kappa}_\infty}{\tilde{\Gamma} \kappa_\infty} = \frac{\Gamma \Delta n}{4 \kappa_\infty \epsilon_0 c \bar{n} n_2}, \quad (\text{A.7b})$$

where we have also used (2.14) and (2.16).

### A.3 Dimensional Experimental Parameters

In terms of the solution to the NLCME, the (scalar, dimensional) electric field is given by

$$E = e_+ e^{ik_B(z-ct/\bar{n})} + e_- e^{-ik_B(z+ct/\bar{n})} + cc$$

where  $cc$  represents the complex conjugate. The mean amplitude of the electric field is thus given by

$$|E|^2 = 2 (|e_+|^2 + |e_-|^2) = 2\mathcal{E}^2 (|E_+|^2 + |E_-|^2),$$

neglecting phase and cross terms. The maximum intensity [3] is

$$I = \frac{1}{2} \epsilon_0 c \bar{n} \max |E|^2 = \epsilon_0 c \bar{n} \mathcal{E}^2 I_{\max}. \quad (\text{A.8})$$

Note that this is a scaling of the nondimensional quantity  $I_{\max}$  defined in (3.2). Combining this with (3.2) and (A.7b),

$$I = \frac{2\Delta n \sqrt{1-v^2}}{n_2(3-v^2)} \sin^2 \frac{\delta}{2} \quad (\text{A.9})$$

Scaling (3.3) by (A.7a) and using that  $\kappa_\infty = \sqrt{\omega^2 + n^2 k^2}$  gives

$$\text{Dimensional FWHM} = \frac{\lambda_B}{\pi \Delta n} \cdot \frac{2\sqrt{1-v^2}}{\sin \delta} \cosh^{-1} \sqrt{1 + \cos^2 \frac{\delta}{2}}.$$

The temporal width is just

$$\text{Dimensional FWHM}_{\text{temporal}} = \frac{\bar{n} \lambda_B}{\pi c \Delta n} \cdot \frac{2\sqrt{1-v^2}}{v \sin \delta} \cosh^{-1} \sqrt{1 + \cos^2 \frac{\delta}{2}}.$$

The coupling function  $\tilde{\kappa}(z)$  has units of inverse length, therefore, the dimensional equivalent of (4.20) scaled by (A.7a) is

$$\Delta_* = \frac{\pi\Delta n}{\lambda_B} \left( 1 - \frac{|\omega|}{\sqrt{\omega^2 + n^2k^2}} \right).$$

The defect width (4.21) scaled by (A.7a) is

$$\text{FWHM} = \frac{\lambda_B}{\pi\Delta n} \cdot \frac{2\sqrt{\omega^2 + k^2n^2}}{k} \tanh^{-1} \left( \frac{\sqrt{2|\omega|\sqrt{\omega^2 + n^2k^2} + n^2k^2 - 2\omega^2}}{2nk} \right).$$

With this information, we can construct the dimensional parameters describing the numerical experiments in Section 6. Table 1 describes the defects and Table 2 describes the gap solitons. For simplicity, all pulse measurements are computed for  $v = 0$  so the spatial width must be used.

Experiment	$\omega$	$k$	$n$	$\Delta_*$ (m <sup>-1</sup> )	Defect FWHM (mm)
1	$\pm 1$	4	1	680	1.6
2.1	-1	2	2	680	3.1
2.2a	-1	1.6	2.5	680	3.9
2.2b	-1	1.33	3	680	4.7

Table 1: Experimental parameters describing the defects in numerical simulations.

Experiment	$\delta$	$I$ (GW · cm <sup>-2</sup> )	Gap Soliton FWHM (mm)
1.1	0.9	490	2.3
1.2	2	1800	1.3
1.3	$\pi/2$	1300	1.5
2.1a	0.9	490	2.3
2.1b	0.6	230	3.4
2.2	0.45	130	4.4

Table 2: Experimental parameters describing the gap solitons in numerical simulations.

## B Defect gratings with a prescribed mode

In this section, we define a simple procedure for generating grating profiles with a given band gap, eigenvalue, and an eigenmode of prescribed shape. We may specify  $\omega$  and look for solutions of the form (see (4.4))

$$\begin{pmatrix} E_+ \\ E_- \end{pmatrix} = e^{-i\omega T} e^{i\sigma_3 \Theta(Z)} f(Z) \begin{pmatrix} v_+ \\ v_- \end{pmatrix} \quad (\text{B.1})$$

where  $v_{\pm}$  are constants,  $\partial_Z \Theta(Z) = V(Z)$ , and  $f(Z)$  is a real scalar function such that  $f(Z) \sim e^{-k|Z|}$  as  $|Z| \rightarrow \infty$ .

Then

$$\frac{\partial E_{\pm}}{\partial Z} = e^{-i\omega T} (f' + iVf) e^{i\Theta(Z)} v_{\pm}.$$

Letting  $g = \frac{f'}{f}$ , this may be rewritten

$$\frac{\partial E_{\pm}}{\partial Z} = (g \pm iV) E_{\pm}.$$

Similarly Then (4.1) becomes

$$(\omega \pm ig)E_{\pm} + \kappa E_{\mp} = 0;$$

By (B.1),

$$\mathcal{L}\vec{v} = \begin{bmatrix} (\omega + ig)e^{i\Theta} & \kappa e^{-i\Theta} \\ \kappa e^{i\Theta} & (\omega - ig)e^{-i\Theta} \end{bmatrix} \begin{pmatrix} v_+ \\ v_- \end{pmatrix} = 0.$$

If (B.1) defines a solution of (4.1) then

$$\det \mathcal{L} = \omega^2 + g^2 - \kappa^2 = 0.$$

Therefore,

$$\kappa(Z) = \sqrt{\omega^2 + g^2(Z)}. \quad (\text{B.2})$$

Note also that if  $f(Z) \sim e^{-k|Z|}$  then  $|g| \rightarrow \pm k$  as  $Z \rightarrow \mp\infty$  and

$$\kappa_{\infty} = \lim_{Z \rightarrow \infty} \kappa(Z) = \sqrt{\omega^2 + k^2}.$$



The width of the gap is then equal to  $2\kappa_\infty$ .

If  $\vec{v}$  is a null eigenvector, then

$$\frac{v_-}{v_+} = -e^{2i\Theta} \frac{\omega + ig}{\kappa}. \quad (\text{B.3})$$

By (B.2), we have that

$$\left| \frac{\omega + ig}{\kappa} \right| = 1$$

and therefore

$$\frac{v_+}{v_-} = e^{i\alpha}, \quad \alpha \text{ real.}$$

Examination of the eventual solution shows that  $\alpha$  merely reflects the invariance of the equations under a constant phase shift. We therefore set  $\alpha = 0$  in the remainder of the argument. Then, in order to satisfy (B.3),

$$2\Theta = \arg \frac{-\omega + ig}{\kappa}.$$

Since  $\kappa$  is positive

$$\Theta = -\frac{1}{2} \arctan \frac{g}{\omega}. \quad (\text{B.4})$$

Then

$$V = -\frac{\omega g'}{2(\omega^2 + g^2)}. \quad (\text{B.5})$$

We may use this method to construct defects that support defect modes of arbitrary shape with prescribed exponential decay. If we choose a function with different exponential decay rates as  $Z \rightarrow \pm\infty$ , then  $\kappa_{\pm\infty}$  will take two different values.

In the case  $\omega = 0$ , we find the same discontinuous limiting behavior as in (4.14). Fortunately, this is merely due to the inadequacy of the polar decomposition implicit in the definition of  $\Theta(Z)$  in (B.1). For  $\omega = 0$ , the entire calculation may be repeated with  $V = 0$ , and a smooth solution generalizing (4.16) is generated:

$$\kappa(Z) = \pm g(Z), \quad (\text{B.6})$$

$$v_- = \mp i v_+. \quad (\text{B.7})$$

## Example

The defect gratings of Section 4.3 which generalize the dark soliton gratings can be obtained as follows. Let

$$f = \operatorname{sech}^n(kZ).$$

Then

$$\kappa(Z) = \sqrt{\omega^2 + n^2 k^2 \tanh^2(kZ)}; \quad (\text{B.8})$$

$$\Theta(Z) = \frac{1}{2} \arctan \frac{nk \tanh(kZ)}{\omega}; \quad (\text{B.9})$$

$$V(Z) = \frac{\omega n k^2 \operatorname{sech}^2(kZ)}{2(\omega^2 + n^2 k^2 \tanh^2(kZ))}. \quad (\text{B.10})$$

And

$$\begin{pmatrix} E_+ \\ E_- \end{pmatrix} = e^{-i\omega t} e^{\pm \frac{i}{2} \arctan \frac{nk \tanh(kZ)}{\omega}} \operatorname{sech}^n(kZ). \quad (\text{B.11})$$

Setting  $n = 1$ , we recover the “dark soliton defect” of Section 4.2. By varying  $n$ , while keeping the quantity  $\omega^2 + n^2 k^2$  fixed, we generate a family of gratings of variable widths with identical band gaps.

Numerical computations indicate that for  $n > 1$ , the system supports multiple eigenmodes obeying the following rule. For  $n > 0$ , the defect supports a total of  $2[n] - 1$  eigenmodes where  $[n]$  is the smallest integer greater than or equal to  $n$ . The ground state has frequency  $\omega_0 = \omega$  and spatial decay rate  $nk$ , whereas the excited states occur in pairs with spatial decay rates given by  $(n - j)k$  and frequencies:

$$\omega_{\pm j} = \pm \sqrt{\omega^2 + (2nj - j^2)k^2} \quad (\text{B.12})$$

for all  $1 \leq j < n$ . It should be possible to derive this formula exactly using methods of complex analysis developed to study bound states of the Schrödinger equation with potential [22], as well as expressions for the associated bound states.

## Acknowledgements

RG was supported by an NSF University-Industry cooperative research fellowship DMS-99-01897. The authors would like to thank Phil Holmes, Vadim

Zharnitsky, Ben Eggleton, and Dmitry Pelinovsky for interesting and informative discussions.

## References

- [1] A. B. Aceves and S. Wabnitz, *Self induced transparency solitons in nonlinear refractive periodic media*, Phys. Lett. A **141** (1989), 37–42.
- [2] G. P. Agrawal, *Nonlinear fiber optics*, second ed., Academic Press, San Diego, 1995.
- [3] ———, *Fiber-optic communication systems*, Wiley–Interscience, 1997.
- [4] I. V. Barashenkov, D. E. Pelinovsky, and E. V. Zemlyanaya, *Vibrations and oscillatory instabilities of gap solitons*, Phys. Rev. Lett. **80** (1998), 5117–5120.
- [5] N. G. R. Broderick and C. M. de Sterke, *Approximate method for gap soliton propagation in nonuniform Bragg gratings*, Phys. Rev. E **58** (1998), 7941–7950.
- [6] N. G. R. Broderick, D. J. Richardson, and M. Ibsen, *Nonlinear switching in a 20-cm-long fiber Bragg grating*, Opt. Lett. **25** (2000), 536–538.
- [7] D. N. Christodoulides and R. I. Joseph, *Slow Bragg solitons in nonlinear periodic structures*, Phys. Rev. Lett. **62** (1989), 1746–1749.
- [8] C. M. de Sterke and J. E. Sipe, *Gap solitons*, Progress in Optics **33** (1994), 203–260.
- [9] B. J. Eggleton, C. M. de Sterke, and R. E. Slusher, *Nonlinear pulse propagation in Bragg gratings*, J. Opt. Soc. Am. B. **14** (1997), no. 11, 2980–2992.
- [10] Z. Fei, Y. S. Kivshar, and L. Vázquez, *Resonant kink-impurity interactions in the  $\phi^4$  model*, Phys. Rev. A **46** (1992), 5214–5220.
- [11] ———, *Resonant kink-impurity interactions in the sine-Gordon model*, Phys. Rev. A **45** (1992), 6019–6030.

- [12] K. Forinash, M. Peyrard, and B. Malomed, *Interaction of discrete breathers with impurity modes*, Phys. Rev. E **49** (1994), 3400–3411.
- [13] R. H. Goodman, P. J. Holmes, and M. I. Weinstein, *Interaction of NLS solitons with defects: Phase space transport in a finite-dimensional model*, (preprint, 2001).
- [14] ———, *Interaction of sine-Gordon kinks with defects: Phase space transport in a two-mode model*, (preprint, 2001).
- [15] R. H. Goodman, M. I. Weinstein, and P. J. Holmes, *Nonlinear propagation of light in one dimensional periodic structures*, J. of Nonlinear Sci. **11** (2001), 123–168.
- [16] A. Hasegawa and F. Tappert, *Transmission of stationary nonlinear optical pulses in dispersive dielectric fibers, I: Anomalous dispersion*, Appl. Phys. Lett. **23** (1971), 142–144.
- [17] B. A. Malomed, *Inelastic interactions of solitons in nearly integrable systems 2*, Physica D **15** (1985), 385–401.
- [18] P. Millar, R. M. De La Rue, T. F. Krauss, J. S. Aitchison, N. G. R. Broderick, and D. J. Richardson, *Nonlinear propagation effects in an AlGaAs Bragg grating filter*, Opt. Lett. **24** (1999), 685–687.
- [19] L. F. Mollenauer, R. H. Stolen, and J. P. Gordon, *Experimental observation of picosecond pulse narrowing and solitons in optical fibers*, Phys. Rev. Lett **45** (1980), 1095–1098.
- [20] H. Rose and M. I. Weinstein, *On the bound states of the nonlinear Schrödinger equation with a linear potential*, Physica D **30** (1988), 207–218.
- [21] G.-H. Song and S.-Y. Shin, *Design of corrugated waveguide filters by the Gel'fand-Levitan-Marchenko inverse scattering method*, J. Opt. Soc. Am. A **2** (1985), 1905–1915.
- [22] E. C. Titchmarsh, *Eigenfunction expansions associated with second-order differential equations. Part I*, Clarendon Press, Oxford, 1962.
- [23] M. I. Weinstein, *Notes on wave propagation in 1-d periodic media with defects*, Tech. report, Bell Labs, 1999.

- [24] V. E. Zakharov and A. B. Shabat, *Exact theory of two-dimensional self-focusing and one dimensional self-modulation of waves in nonlinear media*, Sov. Phys. JETP **34** (1972), 62–69.
- [25] \_\_\_\_\_, *Interaction between solitons in a stable medium*, Sov. Phys. JETP **37** (1973), 823–828.